Journal of Volcanology and Geothermal Research 203 (2011) 12–22

Contents lists available at ScienceDirect

Journal of Volcanology and Geothermal Research

journal homepage: www.elsevier.com/locate/jvolgeores

Tephra fallout hazard assessment for a Plinian eruption scenario at Volcán de Colima (Mexico)

R. Bonasia [a,*], L. Capra [a], A. Costa [b,1], G. Macedonio [b], R. Saucedo [c]

[a] Centro de Geociencias, Universidad Nacional Autonoma de México, Campus Juriquilla, 76230 Queretaro, Mexico
[b] Istituto Nazionale di Geofisica e Vulcanologia, Sezione "Osservatorio Vesuviano", Napoli, Italy
[c] Universidad Autónoma de San Luis Potosí, Instituto de Geología/Fac. Ingenieria, San Luis Potosí, Mexico

ARTICLE INFO

Article history:
Received 19 November 2010
Accepted 23 March 2011
Available online 8 April 2011

Keywords:
volcanic tephra fallout
1913 Colima eruption
Hazmap
hazard assessment
Plinian eruption

ABSTRACT

Volcanic ash fallout associated with renewal of explosive activity at Colima, represents a serious threat to the surrounding urbanized area. Here we assess the tephra fallout hazard associated with a Plinian eruption scenario. The eruptive history of Volcán de Colima shows that Plinian eruptions occur approximately every 100 years and the last eruption, the 1913, represents the largest historic eruption of this volcano. We used the last eruption as a reference to discuss volcanic hazard and risk scenarios connected with ash fallout. Tephra fallout deposits are modeled using HAZMAP, a model based on a semi-analytical solution of the advection–diffusion–sedimentation equation for volcanic particles. Based on a statistical study of wind profiles at Colima region, we first reconstructed ash loading maps and then computed ground load probability maps for different seasons. The obtained results show that a Plinian eruptive scenario at Volcán de Colima, could seriously damage more than 10 small towns and ranches, and potentially affect big cities located at tens of kilometers from the eruptive center. The probability maps obtained are aimed to give support to the risk mitigation strategies.

1. Introduction

Volcán de Colima, located in the western portion of the Trans-Mexican Volcanic Belt, is considered as one of the most active volcanoes in North America, with at least 25 explosive eruptions since 1576 A.D. (De la Cruz Reyna, 1993; Saucedo et al., 2005). Plinian or sub-Plinian events have shown a reoccurrence time of approximately 100 years: starting from 1606, 1690, 1818, and ending with the most recent eruption in 1913. The 1913 eruption, started on the 17th of January and peaked on the 20th of January (Saucedo et al., 2010). It represents the largest historic eruption of Volcán de Colima and it has been used, in literature, as a reference for volcanic hazard and risk scenarios especially focused on pyroclastic flows and lahars (Martin Del Pozzo et al., 1995; Saucedo et al., 2005).

Despite the historic records of Plinian eruptions, and the well documented descriptions of the 1913 event, ash fallout hazard assessments for potential Plinian activity at Colima are still lacking. All emergency and evacuation plans at present do not take into account the risk related to ash fallout associated with a Plinian eruption. Volcanic ash fallout constitutes a serious hazard to communities settled around active explosive volcanoes and the assessment of such hazard is of a great importance for public safety in these regions. The area around the Colima volcano is inhabited by thousands of people. As an example, reconstruction of the 1913 eruption by Saucedo Girón (1997) indicates that along the dispersion axis (NE) the tephra fall deposits had a thickness of approximately 0.45 m at a distance of 8 km and 0.15 m at 26 km in Ciudad Guzmán where many roofs collapsed. Depending on wind conditions, similar ranges of dispersion could be expected for future eruptions of similar magnitude.

Moreover the risk to the Colima area is increased by the perception of risk, which has been heavily influenced by the political and social management rather than the increasing volcanic activity (Gavilanez et al., 2009). (Gavilanez et al., 2009) show that mistakes of risk management have diminished the credibility of authorities and scientists, and people are reluctant to evacuate. For example, people of La Yerbabuena, a little village located south-west of the volcano, do not perceive it to be at risk from the volcano and are reluctant to participate to evacuations plans (Gavilanez et al., 2009).

Therefore, there is a need to improve the information associated with hazards, and here we present a volcanic ash fallout hazard assessment for a Plinian aruption scenario at Colima volcano.

Section 2 describes the stratigraphy and textural characteristics of the 1913 Colima eruption. Section 3 describes briefly the advection–diffusion–sedimentation model for volcanic ash dispersal, HAZMAP (Macedonio et al., 2005). In the first part of Section 4, we reconstruct the deposits produced during the 1913 eruption, and then discuss the

* Corresponding author at: Centro de Geociencias, Universidad Nacional Autonoma de México, Campus Juriquilla, 76230 Queretaro, Mexico.
E-mail address: rbonasia@dragon.geociencias.unam.mx (R. Bonasia).
[1] Now at Environmental Systems Science Centre, University of Reading, Reading, UK.

0377-0273/$ – see front matter © 2011 Elsevier B.V. All rights reserved.
doi:10.1016/j.jvolgeores.2011.03.006

results of statistical analyses of different wind conditions at Colima region. These data allow us to produce several probability maps pivotal for the hazard assessment at the area.

2. Stratigraphical and textural characteristics of the 1913 plinian eruption of volcán de Colima

The 1913 Plinian eruption of Colima has been recently studied by Saucedo et al. (2010). They combined detailed field investigations, eyewitness reports and laboratory analyses to reconstruct the dynamics of the eruption. According to Saucedo et al. (2010), this eruption was produced by a magma mixing event. The authors recognized three main stratigraphic units, described in the composite stratigraphic section shown in Fig. 1. The *Unit 1* consists of four layers, three of which are block-and-ash-flows (F_1 to F_3 in Fig. 1) and the other is a pyroclastic surge (S_1 in Fig. 1).

These block-and-ash-flows are generally comprise by blocks and lapilli clasts that include lithics and scoria in an ash matrix. The pyroclastic surge deposit is a well to moderately sorted stratified bed that contain dark-gray and altered lithics and scoria. *Unit 1* extends as far as 4 km from the vent. *Unit 2* consists of two deposits (S_2 and F_4 in Fig. 1). The first one is a pale-gray to beige pyroclastic surge deposit, widely cross-bedded, although in some places it is massive or shows laminar stratification. The second deposit is a gray massive block-and-ash flow deposit. The authors estimated that this unit is broadly distributed in ravines on the southern flank of the volcano, and extending as far as 12 km from source. *Unit 3* comprises three deposits (C_1, S_3, and F_5 in Fig. 1). C_1 is a beige, clast-supported, pumice-rich fall layer. Saucedo et al. (2010) estimated the maximum preserved thickness to be 1 m at a distance of 2 km, and a minimum reported thickness of <1 mm, in the City of Saltillo, Coahuila, 725 km northeast of the volcano. This deposit is composed of beige to gray pumice lapilli, juvenile lithics, and dark-gray and red altered lithics. According to the authors the C_1 deposit covers an area of ~191,000 km^3. S_3 is a massive to laminar or cross-bedded pyroclastic surge deposit, that is variable in thickness. It is exposed in all the ravines southwards from the crater up to a distance of 9.4 km. The last deposit of the unit (F_5) is an ash and pumice flow deposit. Saucedo et al. (2010) observed that it consists of two or three layers that extends as far as 15 km from the volcano mainly to the south.

In this study we will focus on reconstructing only the deposits associated with ash fallout (i.e. C1 in Fig. 1) using a tephra sedimentation model, described in the next section.

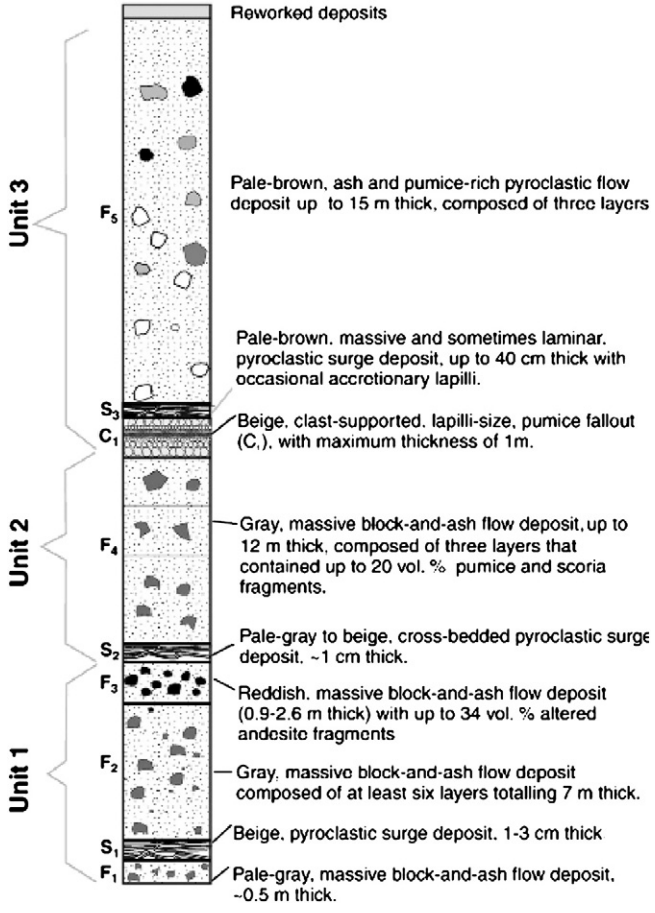

Fig. 1. Composite stratigraphic section of the 1913 Colima eruption (after Saucedo et al. (2010)).

3. The advection–diffusion–sedimentation (ADS) model for volcanic tephra fallout

In order to reconstruct the tephra deposit and constrain the governing eruption parameters needed for producing tephra fallout hazard maps, we used the tephra fallout model HAZMAP (Macedonio et al., 2005). The current version, HAZMAP-2.4 (Macedonio and Costa, 2010), with respect to the original version (Macedonio et al., 2005), includes some changes aimed to improve the performance and to generalize its applicability. In the previous versions of HAZMAP, particle classes were only discerned using settling velocity class, irrespective of their diameter, density and shape. Moreover the variation of the particle settling velocity with height was accounted for using an approximate parameterization, based on the results of (Pfeiffer et al., 2005). In HAZMAP-2.4 particle settling velocities can be calculated directly using several models as function of particle diameters, densities and shapes. The variation of atmospheric properties with altitude is accounted for using a model of the U.S. Standard Atmosphere (1977), which furnishes the air density and viscosity at each elevation.

The HAZMAP model assumes that beyond a certain distance from the eruption column, the dispersion and sedimentation of tephra is governed mainly by wind transport, turbulent diffusion and settling of particles by gravity. Furthermore, it considers that wind field is horizontally uniform, turbulent diffusion is constant, and the vertical wind component and vertical turbulent diffusion are negligible with respect to the horizontal ones (Armienti et al., 1988; Macedonio et al., 2005; Costa et al., 2006; Folch et al., 2009).

Under these hypotheses the concentration of particle class j is described through the mass conservation equation (Macedonio et al., 2005; Pfeiffer et al., 2005):

$$\frac{\partial C_j}{\partial t} + U_x\frac{\partial C_j}{\partial x} + U_y\frac{\partial C_j}{\partial y} - \frac{\partial V_{sj}C_j}{\partial z} = K_x\frac{\partial^2 C_j}{\partial x^2} + K_y\frac{\partial^2 C_j}{\partial y^2} + S_j \quad (1)$$

where C_j denotes concentration of particles class j, t is time, (U_x, U_y) are the horizontal components of the wind velocity vector, K is the horizontal turbulent diffusion coefficients, and V_{sj} and S_j stand for the terminal settling velocity and source term for class j respectively.

Eq. (1) is solved by using a semi-analytical solution as described in (Macedonio et al., 2005) and (Pfeiffer et al., 2005).

A purely empirical description that reproduces the geometrical shape of the eruption column is adopted (Macedonio et al., 2005; Pfeiffer et al., 2005). Then, the source term, in Eq. (1) is described using a modified parameterization proposed by (Suzuki, 1983):

$$S(x,y,z,t) = S_0\left\{\left(1-\frac{z}{H}\right)exp\left[A\left(\frac{z}{H}-1\right)\right]\right\}^{\lambda} \times \delta(t-t_0)\delta(x-x_0)\delta(y-y_0) \quad (2)$$

where S_0 is the normalisation constant, x_0, y_0 are the coordinates of the vent, δ is the Dirac's distribution (i.e. filiform and instantaneous release), H is the column height and A and λ are two empirical

parameters which determine the position of the maximum concentration (located at $H(A-1)/A$) and how closely the mass is concentrated around the maximum (λ).

For further details about the ash transport model see Macedonio and Costa (2010).

One of the limitations of the model is that the parameterization of the eruption column is described as a vertical line. Since this simplification is only really valid far from the vent, the use of the model is limited to areas more than 8 km from the vent. However, as seen in Fig. 3, the model satisfactory reproduced the proximal points within a distance shorter than the height of the eruption column. Another main limitation is associated with the assumption that the wind field is horizontally uniform, which typically holds up to distances of ~100 km (Pfeiffer et al., 2005). Moreover, another reason for restricting the application of this kind of models to distances within few hundred kilometers of the vent is the fact that we do not account for aggregation of fine ashes (Carey and Sigurdsson, 1982; Cornell et al., 1983; Durant et al., 2009; Costa et al., 2010; Folch et al., 2010).

4. Numerical reconstruction of the 1913 Colima tephra fallout deposit and hazard maps based on a plinian scenario

In this section, we describe the methodology used to solve the inverse problem for reconstructing the 1913 Colima eruption fallout deposit and obtaining best fit values for the volcanological and meteo parameters. We also present the results of statistical analysis of different wind profiles for the Colima region and compute representative ash loading maps for each season. These data allow us to produce several probability maps pivotal for hazard assessment for the Colima region.

4.1. Reconstruction of the fallout deposit

Input parameters for the model were taken from best-fitting simulation results and field deposit data from Saucedo et al. (2010). Fitting was performed using a least-squares method comparing measured and calculated deposit thicknesses and grain-sizes (e.g. (Pfeiffer et al., 2005; Costa et al., 2009; Bonasia et al., 2010)). Saucedo et al. (2010) investigated 200 stratigraphic sections around the volcano up to 40 km from the vent. As discussed in Section 3, the computational model used in this work needs stratigraphic sections located at a distances ranging from a minimum (approximately equal to the column height) to a maximum (hundred of kilometers) and fallout beds that can be precisely identified and stratigraphically correlated. For this reason, only 40 stratigraphic sections have been selected (see Fig. 2). All of them are located at a distance of at least 8 km from the vent. Deposit thicknesses measured in Saucedo et al. (2010) were used, and a deposit density of 1070 kg/m^3 was assumed (typical for basalt–andesite tephra fallout deposits (Andronico et al., 2008)).

Component composition and grain-size distribution, used in this work, are those published in Saucedo et al. (2010). In Saucedo et al. (2010), four independent components were recognized, pumice, scoria, lithics and crystals. Measured components density values, reported in Saucedo et al. (2010), are given in Table 1. For this work, for the finer grain-size classes, we calculated a weighted average density of the components of 2070 kg/m^2 using the percentage of each component measured by Saucedo et al. (2010). For the larger grain-size classes (-4 and -3 ϕ), the density value was fixed to the density of the juvenile fragments (see Table 1), which are the most abundant components of these coarser fragments.

For simplicity, empirical parameters appearing in Eq. (2) were fixed assuming $A=4$ and $\lambda=1$. This choice takes into account theoretical and empirical observations of buoyant plumes (e.g., (Morton et al., 1956; Sparks, 1986)), which show that the ratio H_B/H_T between the height of neutral buoyancy of the plume, H_B, and the maximum height, H_T, is usually around 3/4. Previous studies (Macedonio et al., 1988; Pfeiffer et al., 2005; Macedonio et al., 2008; Costa et al., 2009) have shown that for Plinian eruptions these values adequately reproduce the observed tephra deposits.

To reconstruct the tephra fallout from the 1913 eruption, a unidirectional wind profile (Cornell et al., 1983; Carey and Sparks, 1986) was applied. Maximum velocity at the tropopause was found by best-

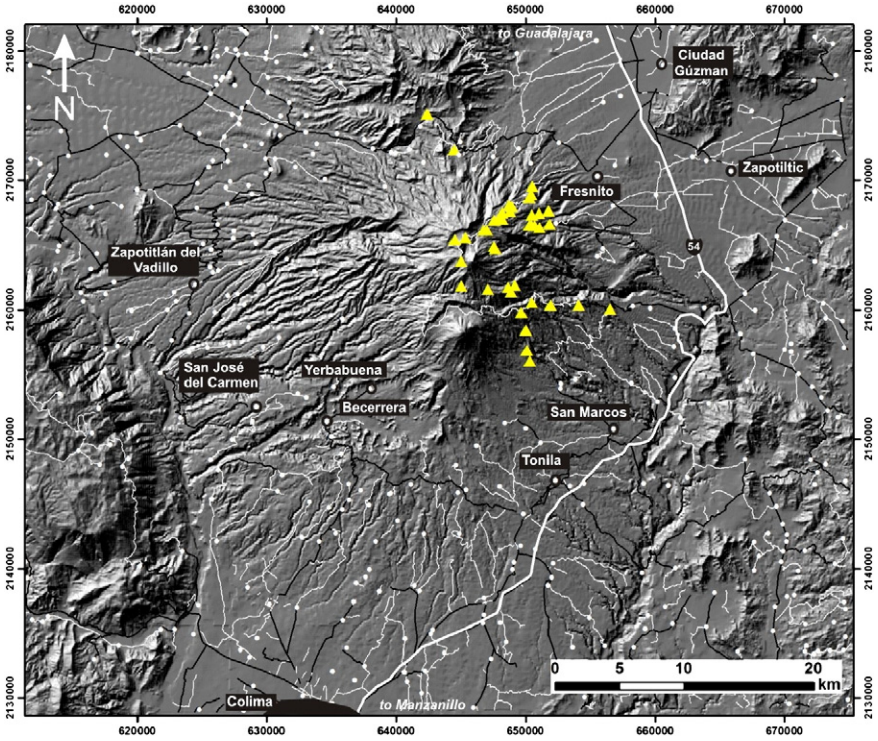

Fig. 2. Location map of the stratigraphic sections. UTM Zone: 13Q. Triangles: sections considered in this work. The map also shows the main highway of the area (indicated with the number 54) that connects the cities of Guadalajara and Manzanillo, the last one of the major harbors of the Pacific Mexican coast, other than minor roads.

Table 1
Density values for the different components.

Component	Density
Pumice	707 kg/m^3
Scoria	1101 kg/m^3
Lithics	2500 kg/m^3
Crystals	2650 kg/m^3

Table 2
Input parameters used to reconstruct the fallout deposit and the ground-load probability maps. Note that wind direction is from E anticlockwise.

Total mass (kg)	2.36×10^{11}
Column height (km)	25
Wind direction at 11 km	64°
Wind speed at 11 km (m/s)	10
Diffusion coefficients (m^2/s)	6500

fit with field data. The direction, also obtained through best fit, was considered to be around the dispersal axis. Results of the fitting procedure are shown in Table 2 and Fig. 3. The total mass of the 1913 eruption was estimated to be 2.36×10^{11} kg, with a column height of about 25 km. A diffusion coefficient value of 6500 m^2/s was obtained and distribution indicates the wind was from the north-east. The reconstructed grain-size distribution (shown in Fig. 4) is depleted in coarse and fine particles. We neglect coarse particles because of the limitations of the model to the very proximal parts of the deposits, and we do not account for very fine ashes because they are only deposited at distances >100 km, where the model is no longer valid (see Section 3).

These values represent the best input parameters, required by HAZMAP to reproduce the deposit of the 1913 Colima eruption (see Fig. 5).

4.2. Wind profile analysis

In order to produce the tephra ground–load probability maps for a Plinian eruption scenario, a wind dataset was extracted from the daily averaged wind profiles corresponding to the point of the NCEP/NCAR global mesh nearest to the Colima volcano, with latitude: 20°N and longitude: 257.5°E, as given by the NCEP/NCAR re-analysis (http://www.cdc.noaa.gov) for the period 1981 to 2009. It comprises 29 years of data with daily values at 17 pressure levels. These levels correspond approximately to vertical levels between ground and 32 km in altitude. The pressure levels were interpolated for every 500 m step

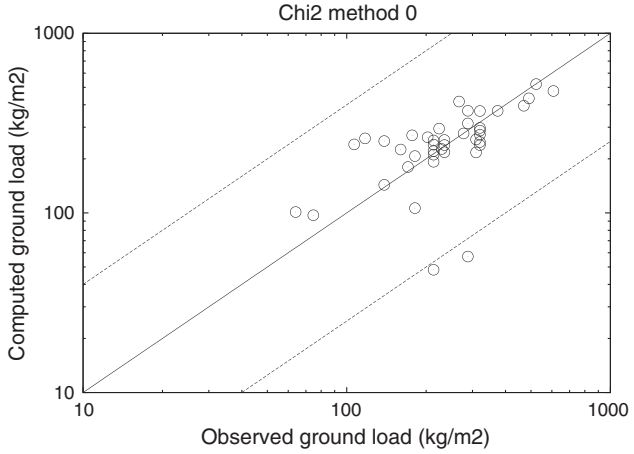

Fig. 3. Log–log plots of the observed tephra deposits (kg/m^2) versus the calculated deposits (kg/m^2). Dotted lines delimit the confidence interval.

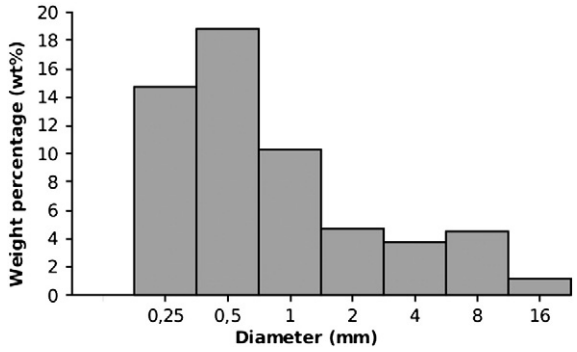

Fig. 4. Total bulk grain-size distribution obtained by best-fit with observed deposit.

in altitude. The statistical distribution at different heights, for the considered period, are reported in Fig. 6.

It shows that below 10 km, during Spring and Autumn, wind directions are almost isotropic. In Winter, the winds are mainly directed towards the east, and during Summer the principal direction is westwards. In this region of the atmosphere, the intensities are always between 0 and 10 m/s. In the high atmosphere (i.e. above 10 km), there is an increase in intensities in almost all the seasons, with the maximum values of 50 m/s, during winter at heights between 10 and 15 km. The effect of increase in intensity higher in the atmosphere is weaker in the Summer, that shows always values between 0 and 10 m/s. Between 10–20 km the atmosphere winds mainly blow from west except in Summer when the main wind direction is westwards. In the interval 20–25 km there is a reduction in wind intensity during all seasons and directions are mainly towards the west.

As discussed above, the statistical distribution of wind intensities and directions (Fig. 6), between 1981 and 2009, indicate that there is a reduction in intensity and an inversion in direction during the Summer. Differences in wind direction are also evident, high in the atmosphere (i.e. between 15 and 25 km), between the Autumn and the other seasons. For these reasons, in order to capture the effect of this seasonal variability on the potential impact of the ash fallout in a Plinian scenario on the area surrounding the Volcán de Colima,

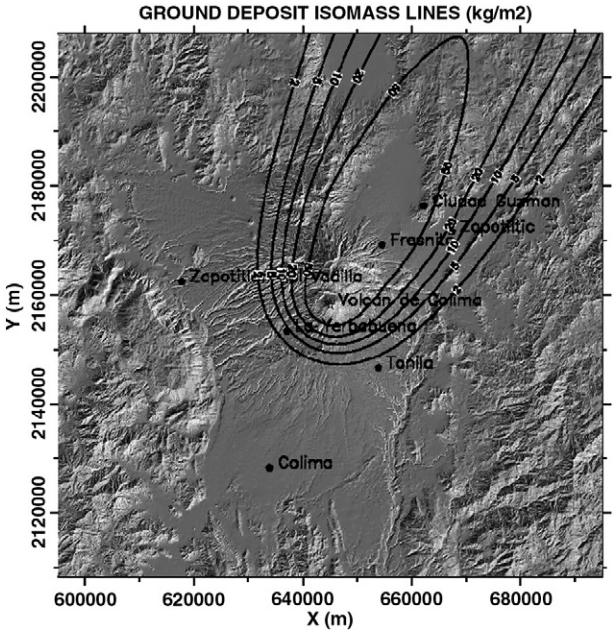

Fig. 5. Fallout deposit of 1913 Colima eruption reconstructed using HAZMAP model with the input values reported in Table 2.

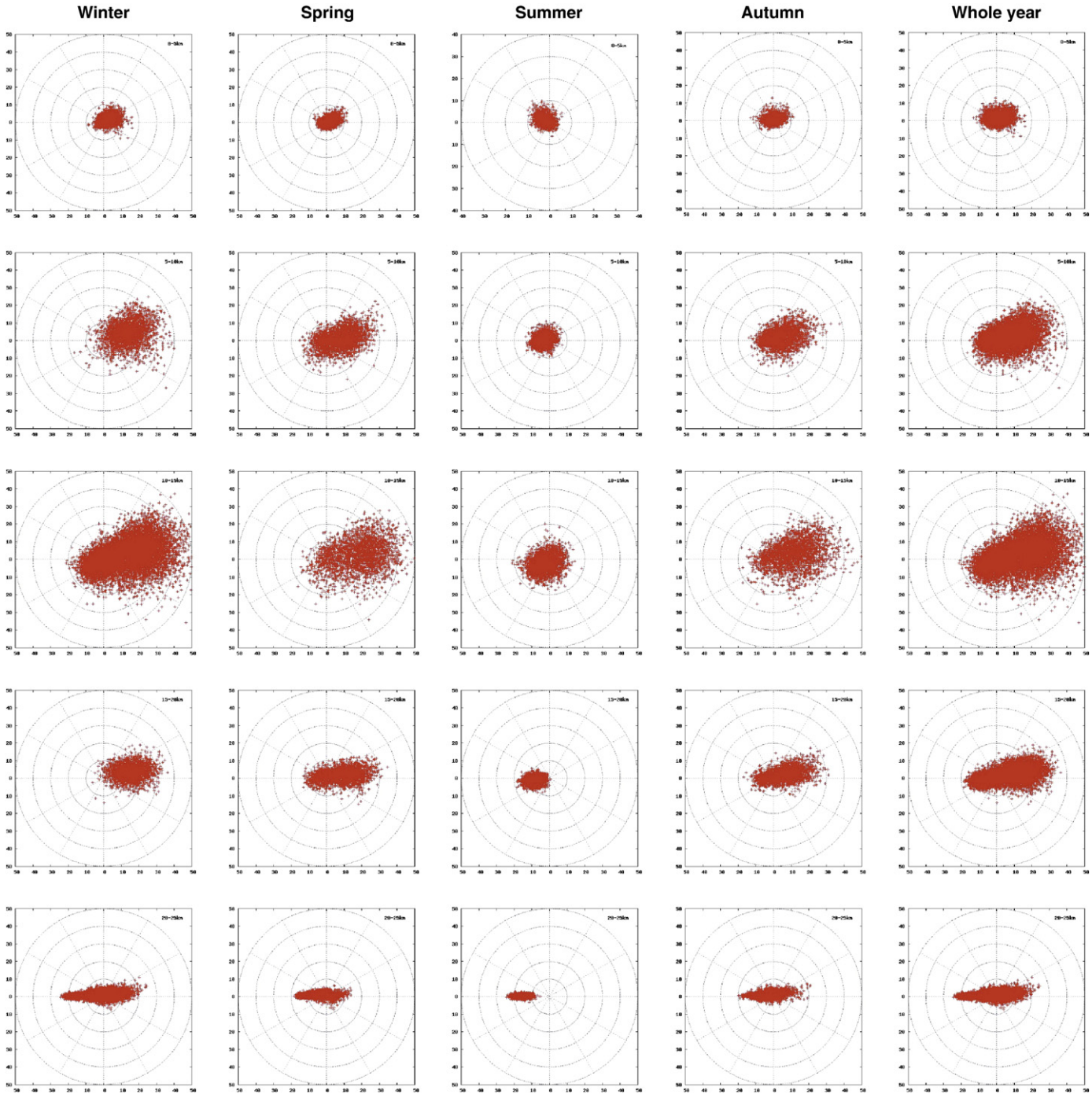

Fig. 6. Wind distribution diagrams corresponding to the point of the NCEP/NCAR global mesh nearest to the Colima volcano (20°N, 257.5°E), for 29 years in the period 1981–2009. Horizontal wind vectors (intensity and direction) are reported at different intervals of height (0–5, 5–10, 10–15, 15–20, 20–25 km respectively).

representative ground load maps for each seasons have been constructed.

As the most representative wind profile for each season, to be used as a input of HAZMAP, we selected the most frequent profile for each season. In order to do that, for each wind profile, we calculated the V_x and V_y velocity components averaged between 0 and 25 km. Then, on the basis of the mean V_x and V_y components, we divided the profiles in velocity classes (this is equivalent to dividing velocity classes on the basis of the mean wind direction and intensity), in regular intervals with a step of 1 m/s. Finally we selected the most frequent wind class for each season. The corresponding wind distributions are quite dispersed (~3 m/s) but all the seasons present a unimodal distribution except for Autumn that has two relative maxima (for this study only the most frequent maximum was considered).

The corresponding tephra ground load maps are shown in Fig. 7.

4.3. Hazard maps

Hazards associated to ash fallout are related to the scale of the eruption. Historic activity of Volcán de Colima has consisted of dome growth and collapse, lava flows and periods of explosive activity, mainly Vulcanian in nature but occasionally Plinian (Saucedo et al., 2005). As we mentioned above, previous to the 1913 eruption, Plinian or sub-Plinian events occurred with a reoccurrence time of approximately

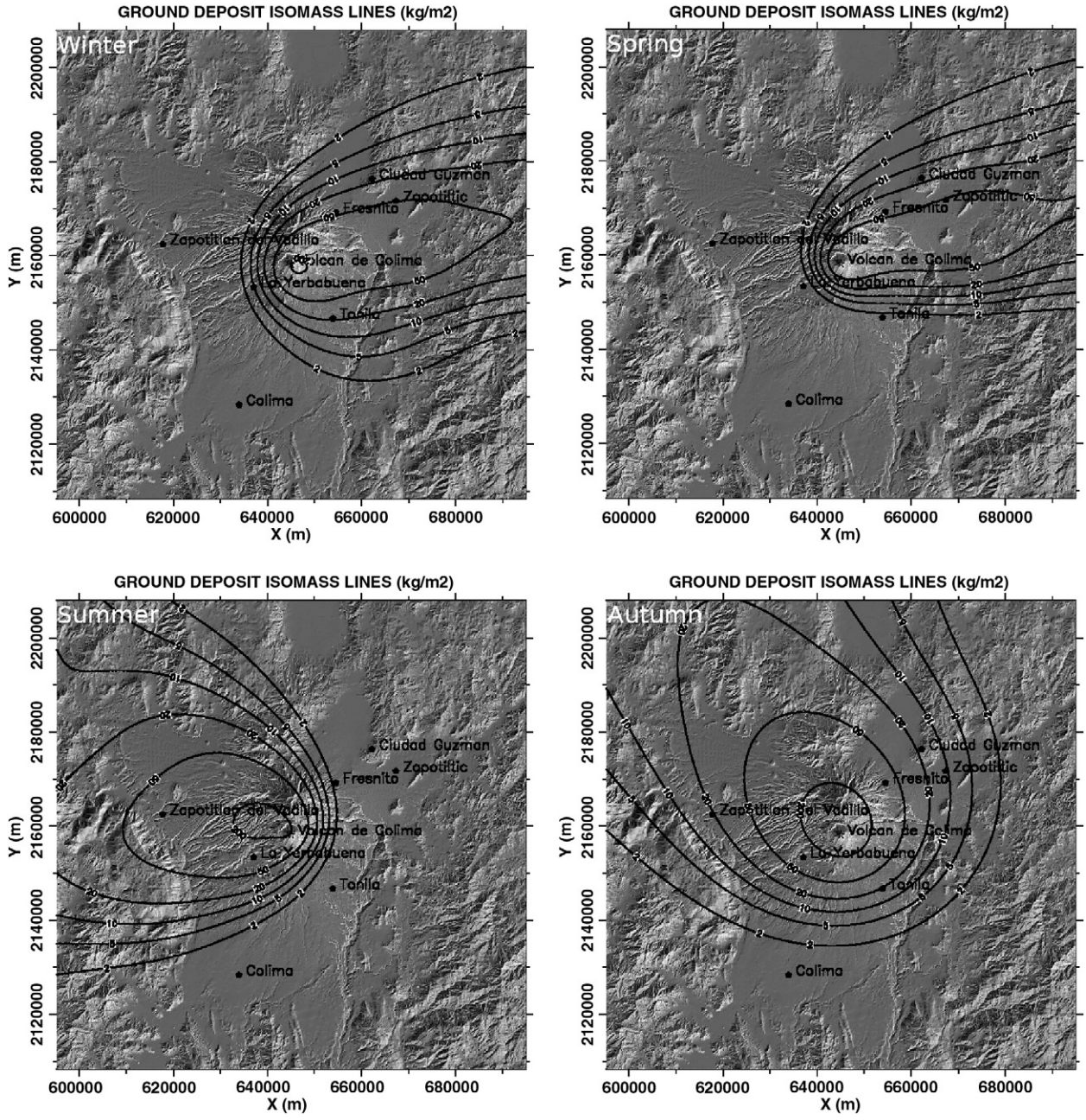

Fig. 7. Isopachs obtained with HAZMAP, relative to each season. The input parameters values used (i.e. column height, total mass and diffusion coefficient) are reported in Table 2. Winds profiles correspond to the most frequent mean winds for seasons in the period between 1981 and 2009.

100 years (Luhr, 2002). This reoccurrence has prompted some scientists to suggest an impending Colima event similar to the 1913 scenario. For these reasons, in the literature, it has been used as a reference for volcanic hazard and risk scenarios, including the construction of hazard maps for pyroclastic flows and lahars (Martin Del Pozzo et al., 1995).

Here, probability maps for the Plinian scenario are obtained using 29 years of daily wind data extracted from NCEP/NCAR Reanalysis database (i.e. 365 (or 366) days times 29 years in the period 1981–2009 = 10950 HAZMAP runs). Input parameters relative to the eruptive scenario were obtained solving the inverse problem to reproduce the ash deposit of the 1913 eruption (see Section 4.1). Moreover, because there are seasonal variations in wind distributions (see Fig. 6), hazard maps relative to each season are also reported. We computed ash loading probability maps for several thresholds values from 100 to 500 kg/m^2. Here we present only maps for loading thresholds of 100 and 200 kg/m^2. Maps with thresholds greater than 200 kg/m^2 are very proximal and do not affect inhabited areas or viability. According to (Baxter, 1999), loadings of 200 kg/m^2 are considered critical for long-span roof collapse of low quality buildings. Moreover, loadings of 200 kg/m^2 can collapse roofs even in high quality buildings, which, in turn, may cause direct impact injury with impact to the skull and the body, and the inflow of ash may partially bury and/or suffocate people (Baxter, 1999).

Fig. 8 shows the probability maps obtained for the Plinian scenario, for loadings of 100 and 200 kg/m^2, using 29 years of daily winds irrespective of season. Fig. 9 shows ash loading probability maps calculated for the different seasons of the year.

The risk to infrastrucures in proximal areas is high. Roof collapse is not the only threat. A few millimeters of ash blanketing a large area, even tens of kilometers from the vent, could cause airport disruption and/or the interruption of the crucial communication networks. To establish if this threat would affect the Colima region, we also

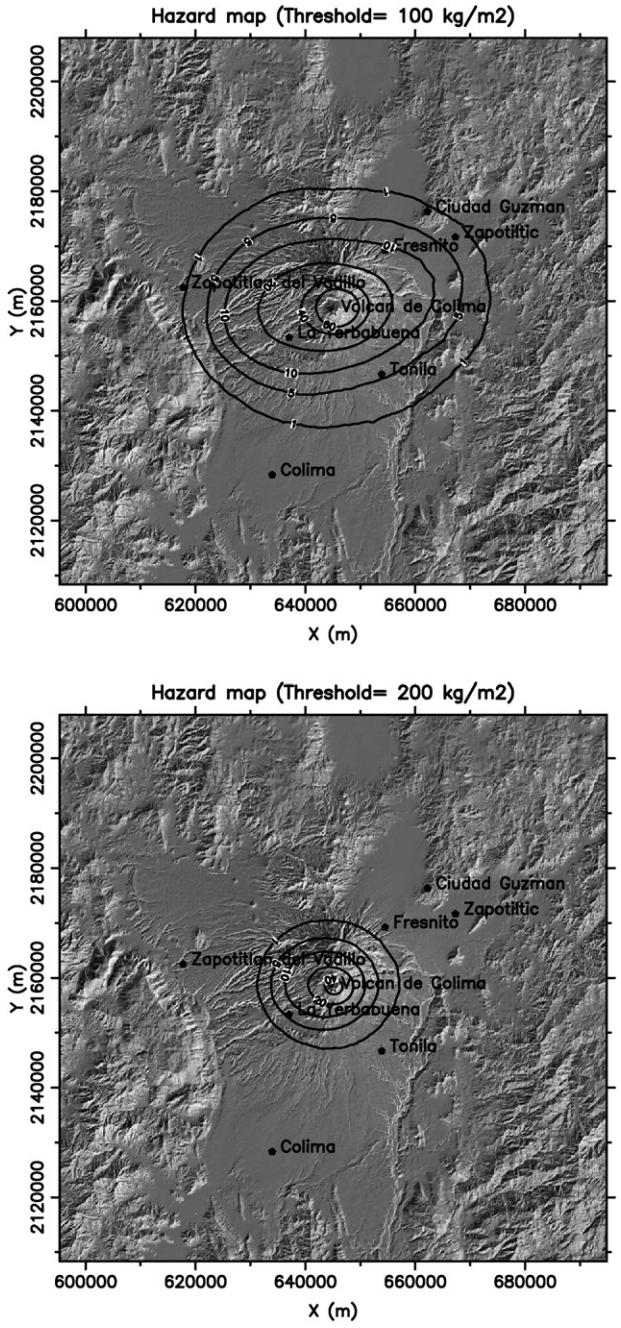

Fig. 8. Ash loading probability maps for a Plinian scenario. Top: 100 kg/m^2, bottom: 200 kg/m^2.

constructed seasonal ash loading probability maps for the lower threshold of 10 kg/m^2. These probability maps are shown in Fig. 10.

5. Summary and discussion

The fit obtained using the least squares method, for the reconstruction of the 1913 Colima eruption, produced results in agreement with those of Saucedo et al. (2010) using classical methods.

A maximum eruption column height of 25 km was predicted by the model, which is to that calculated by Saucedo et al. (2010), 23 km, using the method of (Carey and Sparks, 1986).

For what concerns the wind direction, the main distribution axis can be defined at a north-easterly direction.

The total mass value found is 2.361×10^{11} kg. Saucedo et al. (2010) calculated a value for total mass of 1.5×10^{12} kg, with the methods of Pyle, (1989) and Fierstein and Nathenson (1992). It is worth noting that in our simulations we excluded the coarsest and the finest particle populations because of the model limitations. By comparing our result with the measurement of the volume relative to the proximal slope only in the diagram of thickness vs. the square root of the area of the 1913 fall deposit, (Fig.9 in Saucedo et al., 2010), the results show that the values are very close one to the other.

In summary our simulations satisfactorily reproduced the actual 1913 fallout deposit and are in good agreement with the isopachs drawn by Saucedo et al. (2010) (see Fig.8.A in (Saucedo et al., 2010)).

Using the input parameters obtained by the inversion method (reported in Table 2) and the most frequent wind profile for each season, we extracted a statistical set of re-analysis wind profiles, and have constructed representative ash load maps for different seasons (Fig. 7). Winter and Spring winds typically disperse, and create ash loadings, east of the volcano. While, ash deposit during Winter would probably affect a wider area: the densely inhabited towns like Ciudad Guzmán (NE of the volcano) and Tonila (SE), smaller inhabited localities and the N.54 highway. A similar scenario would occur during Spring. The slightly more intense winds produce tight isopachs, mainly directed to the north and the east, without affecting the city of Tonila. During the Summer there is an inversion in wind direction and a reduction intensity. Thus, isopachs are widespread towards the west, producing ash loading, that would affect small inhabited localities with more than 8000 inhabitants. During the Autumn the ash deposit would affect a wide area including more than 23,000 inhabitants and the main highway and provincial roads.

Using the same input parameters of Table 2 and a statistical set of re-analysis wind profiles (more than 10,000), we have constructed tephra loading probability maps for several thresholds from 100 to 500 kg/m^2. Loading thresholds of 100 and 200 kg/m^2 (Fig. 8) are presented and discussed. Probability maps with a loading of 100 kg/m^2 involve a wide area that extends almost symmetrically east and west. In this map, the lower probability value (1%) involves an area that extends roughly over 535 km^2, and affects the city of Tonila (SE). Higher probability values (e.g. 10%) affect an area of ~200 km^2, including little villages close to the volcano. Maps with the loading of 200 kg/m^2, show that only a localised area may be affected.

Moreover, in order to define a different impact on the area surrounding the volcano during different periods of the year, ash loading probability maps for all four seasons have been constructed (Fig. 9a, b, c and d). During the Winter the ash dispersal is mainly towards the east. The 1% of probability that the ash loading overcome a threshold of 100 kg/m^2 involves an area of 320 km^2, comprised between the localities of La Yerbabuena (south-west of the volcano) and Fresnito (north-east of the volcano). Higher probability values (e.g. 5%), still affect a quite wide area roughly 150 km^2. The map with loading value 200 kg/m^2, affect a very short area close to the volcano. Ground load probability maps obtained for Spring show that areas enclosed by the threshold of 100 kg/m^2, for the larger probability case (from 10 to 60%), are mainly directed eaststwards, and involve an area of 150 km^2. Lower probabilities (<10%) involve a bigger area (roughly 290 km^2), towards the western, affecting the localities of La Yerbabuena and Bercerrera (both south-west of the volcano). The map with loading value 200 kg/m^2, again involve a restricted area around the volcano, which still affect the little village of La Yerbabuena. For what concerns the Summer, winds are mainly directed westwards. Thus, hazard maps involve a wide area that extends to the west of the volcano. The maps show that there is a high probability to overcome the loading threshold of 100 kg/m^2 up to the localities of La Yerbabuena and Bercerrera. Moreover, there is a 1% probability that a loading of 100 kg/m^2 will be overcome, which would affect the city of Tonila (south-east of the volcano). During Summer, La Yerbabuena is enclosed by the 1% probability curve to

exceed the threshold value of 200 kg/m^2. During the Autumn, the 1 and 5% probability curves to overcome the threshold value of 100 kg/m^2 involve a relatively wide area around the volcano that extends towards both the east and the west. This ash load, affects small villages, like Bercerrera and La Yerbabuena (south-west of the volcano), and big towns like Tonila (south-east of the volcano). Higher loadings, i.e. 200 kg/m^2, affect a smaller area around the volcano, and still involves the little village of La Yerbabuena.

As mentioned in the previous section, roof collapse is not the only hazard associated with ash fallout. Accumulation of fine ash can also interrupt lifelines (roads, railways, etc.), disrupt airport operations, and damage to communications. Moreover, the accumulation of few millimeters (ash load of about 10 kg/m^2) is sufficient to cause airport disruption or closure. In order to assess the impact of very fine ash over the Colima region, probability maps with load exceeding the threshold value of 10 kg/m^2 were also constructed (Fig. 10). However, application to very fine ash represents an extrapolation of the model application as for a more rigorous description of the very fine ash aggregation process should be accounted for (see e.g. (Costa et al., 2010; Folch et al., 2010)).

The maps show that the probability of an ash loading during any season, that would affect the city (10 kg/m^2), and its airport, is 1% to 20%. Furthermore, a wide area to the north-east of the volcano could be affected, 20 to 60% probability, if the loading threshold of 10 kg/m^2 is exceeded. This area, is crossed by the highway N.54 (see Fig. 2), which is an important connection between the cities of Guadalajara and Manzanillo, one of the most important harbors along the Pacific Mexican coast.

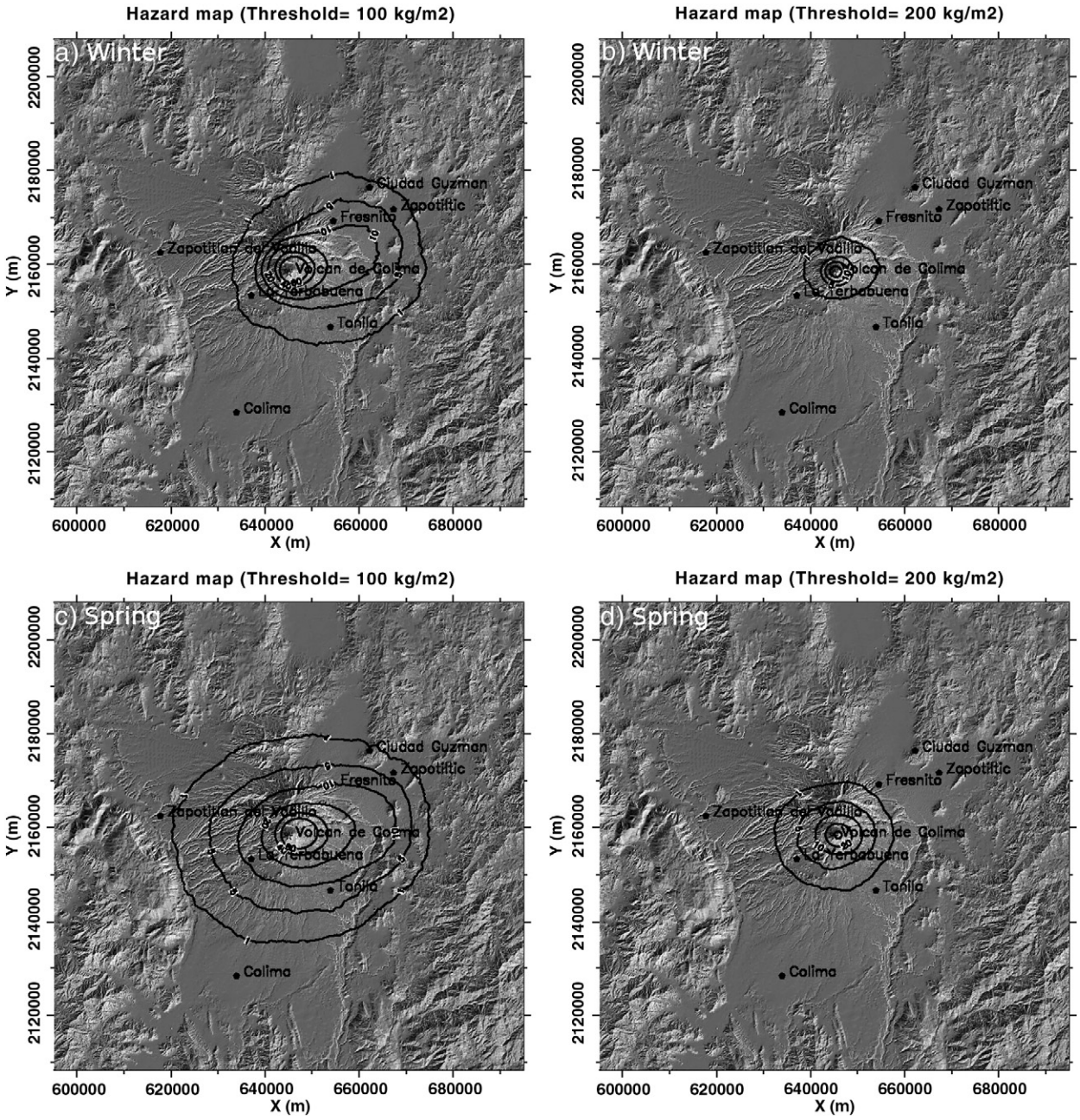

Fig. 9. Ash loading probability maps for Plinian scenario, during the four seasons. a) and b): Winter; threshold values 100 kg/m^2 (left) and 200 kg/m^2 (right). c) and d): Spring; threshold values 100 kg/m^2 (left) and 200 kg/m^2 (right). e), f): Summer; threshold values 100 kg/m^2 (left) and 200 kg/m^2 (right). g), h): Autumn; threshold values 100 kg/m^2 (left) and 200 kg/m^2 (right).

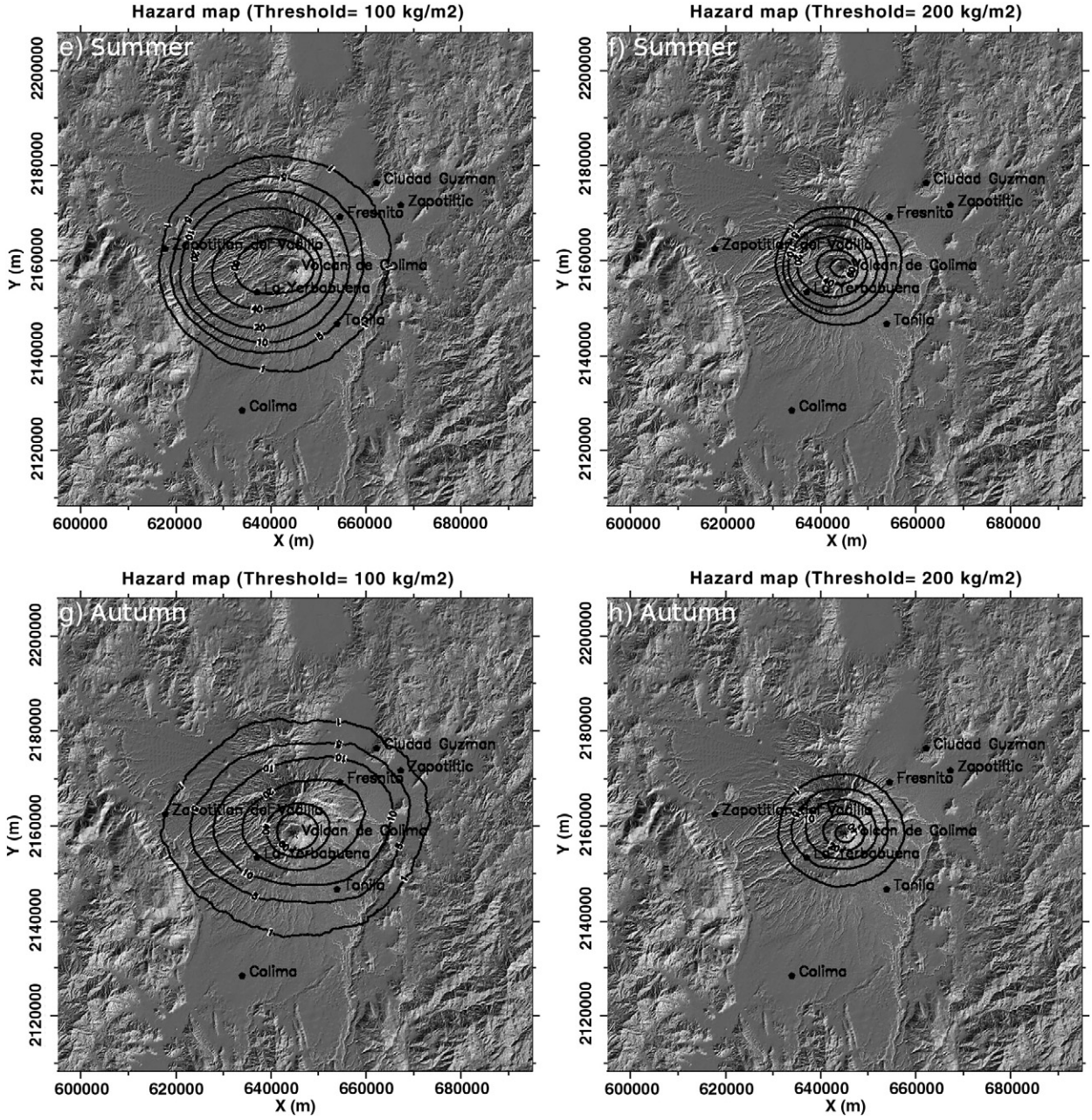

Fig. 9 (*continued*).

6. Conclusions

A methodology that solves an inverse problem, using a semi-analytical ash fallout model has reconstructed ash fallout deposition from the 1913 Colima eruption. These new results are in good agreement with previous estimations carried out using classical methods by Saucedo et al. (2010).

Statistical analysis of different wind profiles for the Colima region, extracted from a 29 year long NCEP/NCAR re-analysis wind dataset (1981 and 2009) of daily averaged values show a marked seasonal variation in both wind intensity and direction.

The simulated scenario provides evidence that a future Plinian eruption at Colima Volcano, depending on the main wind direction, would cause significant damage to buildings and infrastructures, and affect big cities like Tonila and Ciudad Guzmán, and smaller inhabited localities like La Yerbabuena and Fresnito. Moreover, a few millimeters of deposition around the volcano would seriously threaten air and road traffic and potentially affect the Colima airport and rad network (probability 1 and 60%).

The existing hazard map for Colima Volcano (Navarro et al., 2003) displays a circular area that can be affected by ash fallout and does not quantify ash thickness or the probability of exceeding dangerous loading threshold values. These data are crucial to estimate the associated risk. Thus, this work represents an helpful contribution to the hazard assessment for a Plinian eruption scenario at Volcán de Colima, in case of renewal of explosive activity.

Acknowledgements

The authors would like to thank Arnau Folch and Roberto Sulpizio for constructive reviews of this manuscript. NCEP-Reanalysis 2 data were provided by the NOAA/OAR/ESRL PSD, Boulder, Colorado, USA,

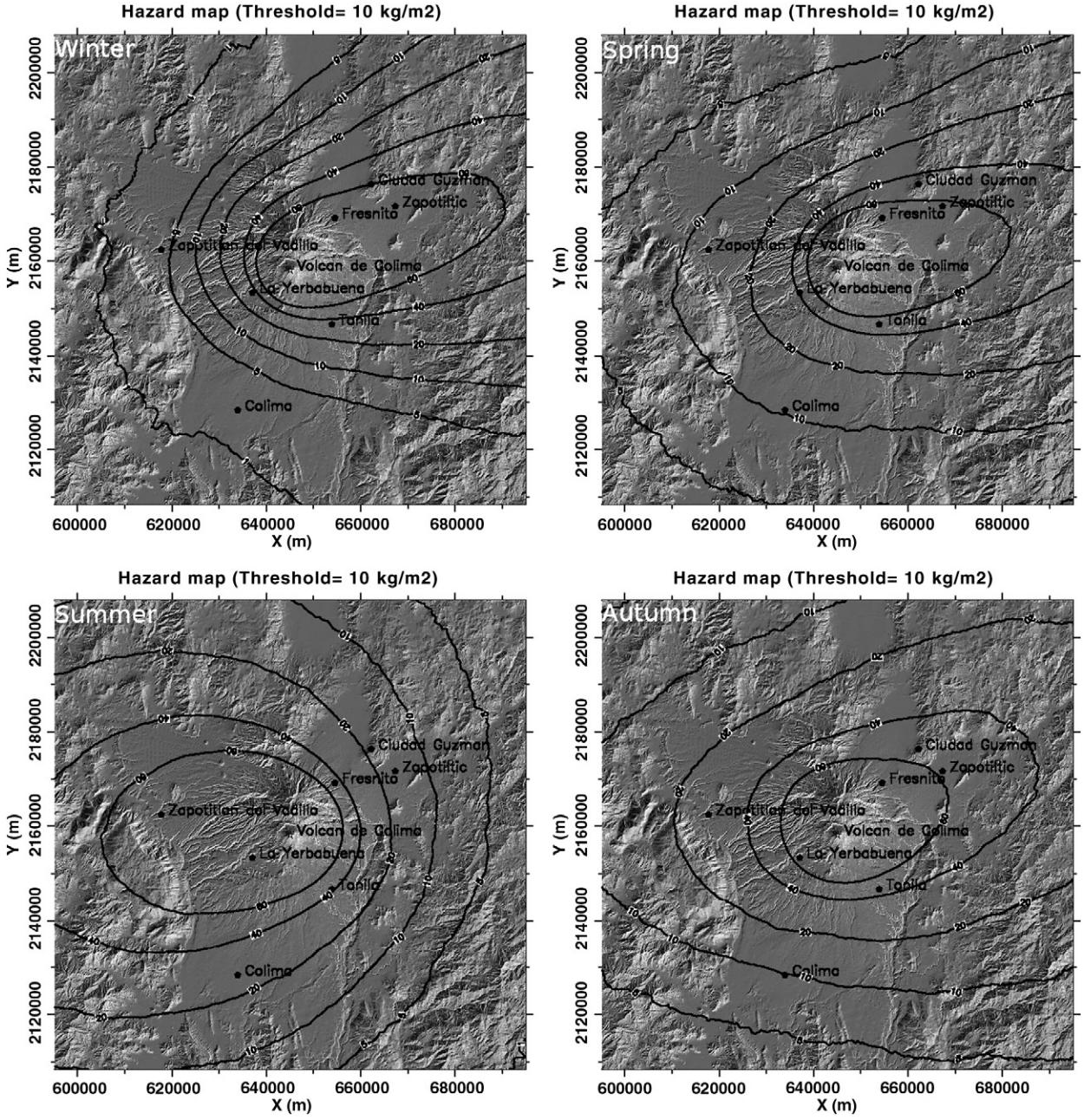

Fig. 10. Ash loading probability maps for the threshold value 10 kg/m^2, for a Plinian scenario, during the four seasons.

from their Web site at http://www.esrl.noaa.gov/psd/. R. Peluso is also acknowledged for his helpful computer support. We are grateful to V. C. Smith for correcting the English. This work was mainly supported by the CONACYT Project no. 99486 (Lucia Capra).

References

Andronico, D., Scollo, S., Caruso, S., Cristaldi, A., 2008. The 2002–2003 Etna explosive activity: tephra dispersal and features of the deposits. J. Geophys. Res. 113, B04209 10.29/2007JB005126.

Armienti, P., Macedonio, G., Pareschi, M., 1988. A numerical model for simulation of tephra transport and deposition: application to May 18, 1980 Mount St. Helens eruption. J. Geophys. Res. 93 (B6), 6463–6476.

Baxter, P., 1999. Encyclopedia of volcanoes. Academic, San Diego, California, Ch. Impacts of eruptions on human health, pp. 1035–1043.

Bonasia, R., Macedonio, G., Costa, A., Mele, D., Sulpizio, R., 2010. Numerical inversion and analysis of tephra fallout deposits from the 472 AD sub-Plinian eruption at Vesuvius (Italy) through a new best-fit procedure. J. Volcanol. Geotherm. Res. 189, 238–246. doi:10.1016/j.jvolgeores.2009.11.009.

Carey, S., Sigurdsson, H., 1982. Influence of particle aggregation on deposition of distal tephra from the May 18, 1980, eruption of Mount St-Helens volcano. J. Geophys. Res. 87 (B8), 7061–7072.

Carey, S., Sparks, R., 1986. Quantitative models of the fallout and dispersal of tephra from volcanic eruption columns. Bull. Volcanol. 48, 109–125.

Cornell, W., Carey, S., Sigurdsson, H., 1983. Computer simulation and transport of the Campanian Y-5 ash. J. Volcanol. Geotherm. Res. 17, 89–109.

Costa, A., Dell'Erba, F., Di Vito, M., Isaia, R., Macedonio, G., Orsi, G., Pfeiffer, T., 2009. Tephra fallout hazard assessment at Campi Flegrei caldera (Italy). Bull. Volcanol. 71 (3), 259–273.

Costa, A., Folch, A., Macedonio, G., 2010. A model for wet aggregation of ash particles in volcanic plumes and clouds: 1. Theoretical formulation. J. Geophys. Res. 15 (B09201).

Costa, A., Macedonio, G., Folch, A., 2006. A three-dimensional Eulerian model for transport and deposition of volcanic ashes. Earth Planet. Sci. Lett. 241, 634–647.

De la Cruz Reyna, S., 1993. Random patterns of occurrence of explosive eruptions at Colima Volcano, México. J. Volcanol. Geotherm. Res. 55, 51–68.

Durant, A., Rose, W., Sarna-Wojcicki, A., Carey, S., Volentik, A., 2009. Hydrometeor-enhanced tephra sedimentation: constraints from the 18 May 1980 eruption of Mount St. Helens. J. Geophys. Res. 114 (B13).

Fierstein, J., Nathenson, M., 1992. Another look at the calculation of tephra fallout volumes. Bull. Volcanol. 54, 156–167.

Folch, A., Costa, A., Durant, A., Macedonio, G., 2010. A model for wet aggregation of ash particles in volcanic plumes and clouds: 2. Model application. J. Geophys. Res. 115 (B09202).
Folch, A., Costa, A., Macedonio, G., 2009. FALL3D: a computational model for transport and deposition of volcanic ash. Comput. Geosci. 35 (6), 1334–1342.
Gavilanez, J., Cuevas, A., Varley, N., Gwynne, G., Stevenson, J., Saucedo, R., Pérez, A., Aboukhalil, M., Cortés, A., 2009. Exploring the factors that influence the perception of risk: the case of Volcán de Colíma, Mexico. J. Volcanol. Geotherm. Res. 186, 238–252.
Luhr, J., 2002. Petrology and geochemistry of the 1991 and 1998–1999 lava flows from Volcán de Colíma, Mexico: implications for the end of the current eruptive cycle. J. Volcanol. Geotherm. Res. 117 (1–2), 169–194.
Macedonio, G., Costa, A., 2010. HAZMAP-2.4 User Manual. Istituto Nazionale di Geofisica e Vulcanologia. Sezione "Osservatorio Vesuviano", Via Diocleziano 328–80124 Napoli, Italy.
Macedonio, G., Costa, A., Folch, A., 2008. Ash fallout at Vesuvius: numerical simulations and implication for hazard assessment. J. Volcanol. Geotherm. Res. 178, 366–377.
Macedonio, G., Costa, A., Longo, A., 2005. A computer model for volcanic ash fallout and assessment of subsequent hazard. Comput. Geosci. 31, 837–845.
Macedonio, G., Pareschi, M., Santacroce, R., 1988. A numerical simulation of the Plinian fall phase of 79 AD eruption of Vesuvius. J. Geophys. Res. 93, 14817–14827.
Martin Del Pozzo, A., Sheridan, M., Barrera, D., Hubp, J., Selem, L., 1995. Potential Hazards from Colima Volcano, Mexico. Geof. Intern. 34, 363–373.
Morton, B., Taylor, G., Turner, S., 1956. Turbulent gravitational convection from maintained and instantaneous sources. Proc. R. Soc. Lond 234, 1–23.
Navarro, C., Cortés, A., Téllez, A., 2003. Mapa de peligros del Volcán de Fuego de Colima. Universidad de Colima, México, scale 1:100,000, 1 Sheet.
Pfeiffer, T., Costa, A., Macedonio, G., 2005. A model for the numerical simulation of tephra fall deposits. J. Volcanol. Geotherm. Res. 140, 237–294.
Pyle, D., 1989. The thickness, volume and grainsize of tephra fall deposits. Bull. Volcanol. 51, 1–5.
Saucedo, R., Macías, J., Gavilanez, J., Arce, J., komorowski, J., Gardner, J., Valdez-Moreno, G., 2010. Eyewitness, stratigraphy, chemistry, and eruptive dynamics of the 1913 Plinian eruption of Volcán de Cólima, México. J. Volcanol. Geotherm. Res. 101, 149–166.
Saucedo, R., Macias, J., Sheridan, M., Bursik, M., Komorovski, J., 2005. Modeling of pyroclastic flows of Colima Volcano, Mexico: implication for hazard assessment. J. Volcanol. Geotherm. Res. 139 (1–2), 103–115.
Saucedo Girón, R., 1997. Reconstrucción de la erupción de 1913 del Volcán de colíma. Master's thesis, Instituto de Geofisica, UNAM, Mexico.
Sparks, R., 1986. The dimensions and dynamics of volcanic eruption columns. Bull. Volcanol. 48 (1), 3–15.
Suzuki, T., 1983. A theoretical model for dispersion of tephra. In: Shimozuru, D., Yokoyama, I. (Eds.), Volcanism: Physics and Tectonics. Terrapub, Tokyo, pp. 95–113.